land

MDPI

Article

Modelling the Control of Groundwater on the Development of Colliery Spoil Tip Failures in Wales

Lingfeng He [1,2,*], John Coggan [2], Patrick Foster [2], Tikondane Phiri [2] and Matthew Eyre [2]

[1] Hangzhou International Innovation Institute, Beihang University, Hangzhou 311115, China
[2] Camborne School of Mines, Penryn Campus, University of Exeter, Penryn TR10 9EZ, UK; j.coggan@exeter.ac.uk (J.C.); p.j.foster@exeter.ac.uk (P.F.); tp501@exeter.ac.uk (T.P.); m.eyre@exeter.ac.uk (M.E.)
* Correspondence: lingfeng_he@buaa.edu.cn

Abstract: Legacy colliery spoil tip failures pose a significant hazard that can result in harm to persons or damage to property and infrastructure. In this research, the 2020 Wattstown tip landslide caused by heavy rainfall was examined to investigate the likely mechanisms and developmental factors contributing to colliery spoil tip failures in Welsh coalfields. To achieve this, an integrated method was proposed through the combination of remote sensing mapping, stability chart analysis, 2D limit equilibrium (LE) modelling, and 3D finite difference method (FDM) analysis. Various water table geometries were incorporated into these models to ascertain the specific groundwater condition that triggered the occurrence of the 2020 landslide. In addition, sensitivity analyses were carried out to assess the influence of the colliery spoil properties (i.e., cohesion, friction angle, and porosity) on the slope stability analysis. The results indicate that the landslide was characterised by a shallow rotational failure mode and spatially constrained by the critical water table and an underlying geological interface. In addition, the results also imply that the landslide was triggered by the rise of water table associated with heavy rainfall. Through sensitivity analysis, it was found that the properties of the colliery spoil played an important role in confining the extent of the landslide and controlling the process of its development. The findings underscore the detrimental effects of increased pore pressures, induced by heavy rainfall, on the stability of colliery tips, highlighting the urgent needs for local government to enhance water management strategies for this region.

Keywords: colliery spoil; landslide; groundwater; 3D finite difference method; numerical modelling

Citation: He, L.; Coggan, J.; Foster, P.; Phiri, T.; Eyre, M. Modelling the Control of Groundwater on the Development of Colliery Spoil Tip Failures in Wales. *Land* **2024**, *13*, 1311. https://doi.org/10.3390/land13081311

Academic Editor: Fabrizio Terenzio Gizzi

Received: 30 May 2024
Revised: 13 August 2024
Accepted: 15 August 2024
Published: 19 August 2024

1. Introduction

A spoil tip refers to a pile of discarded rock and soil removed during historic mining operations, which is composed of various-sized particles upwardly grading from fine silt to large boulders. Historic tips were generally formed in an uncontrolled manner by loose tipping and were geometrically characterised as conical or irregular in shape with a high profile in relation to the local topography [1]. In addition, long-term rehabilitation or stabilisation actions for visually stable spoil tips may not have occurred. As a consequence, legacy spoil tips pose a significant hazard and potential instability resulting from external disturbance or changes in equilibrium, such as increased pore pressure associated with an influx of water or dynamic loading associated with seismicity.

According to a recent investigation, Wales has 2456 disused colliery spoil tips of which 327 are regarded as posing a high potential safety risk [2]. Historic failures of spoil tips have occurred in this region, with several reported in the review undertaken by [3]. The Aberfan disaster, which caused the collapse of a National Coal Board spoil tip near the village of Aberfan, engulfed a junior school and a row of houses and killed 116 children and 28 adults. More recently, the Tylorstown landslide blocked the river valley, broke a foul sewer, covered a strategic water main with several metres of debris, and covered a footpath and cycle path [4]. The 2020 Wattstown landslide, which was spatially located close to

Tylorstown (3 km S.S.E. of Tylorstown landslip) highlights the safety concerns posed for the immediate area.

As man-made slopes, spoil tips are subject to a range of factors that can impact their stability. Among these factors, soil material is recognised as playing a decisive role in determining soil mechanical properties. Since spoil tips are generally composed of rock–soil mixtures, the mechanical behaviour of these heterogeneous media is highly influenced by the nature of spoils [5], proportion of rock content [6,7], and structural properties [8]. In addition, soil porosity is another critical factor for tip stability that is dependent on the interplay of particle size, soil gradation [9], particle shape, and compressibility [10,11]. From a hydrogeological prospective, soil with high porosity is capable of storing more water content, inducing excessive levels of pore water pressure in saturated conditions [12]. The above-mentioned soil-related factors can be regarded as internal factors that can influence the stability of a spoil tip.

In terms of external factors, rainfall or increases in the water table are regarded as one of the most significant factors. Various slope instability or landslide events have demonstrated that rainfall, particularly extreme rainfall events, can cause a rise in the water table and associated pore water pressure, which can lead to the initiation of shallow failures and subsequent debris flows [13–15]. In addition, debuttressing can trigger or initiate landslides. This occurs when the support at the toe of slopes is lost due to water erosion [16,17], deglaciation [18,19], or anthropogenic excavation [20,21]. Earthquakes or seismic activity may also trigger for landslides through which the transmission of seismic waves causes the shaking and vibration of a ground surface [22,23].

In order to assess the stability of soil slopes, stability chart approaches are commonly employed to provide a preliminarily estimate of the factor of safety (FS) for a slope that may be susceptible to circular or rotational failure. These include the Hoek and Bray chart solution [24], Taylor's chart solution [25], Bishop solution [26], and Spencer solution [27]. However, such chart solutions have several limitations, including their inability to account for irregular slope geometry, complicated scenarios of groundwater distributions, stress and displacement problems, and heterogeneous materials. To overcome these limitations, advanced numerical methods have been developed that take into consideration the slope geometry, water table and rock/soil properties. For example, numerical limit equilibrium (LE) approaches, such as Slide2 and Slide3, can be used to estimate the slope FS (factor of safety) and undertake groundwater sensitivity analyses, as well as to assess potential remediation or stabilisation strategies [28–30]. However, these approaches are limited in their ability to model complex structures and interactions of soil and structures, which has led to the preference for continuum numerical modelling approaches (e.g., finite-difference methods, FDMs) [31]. Continuum approaches are able to accommodate a wide range of soil behaviour and capture pore water pressure effects effectively [32–35].

The primary aim of this research is to investigate the mechanism and development of the 2020 Wattstown tip landslide. This is achieved by utilising different analysis methods, including the use of stability charts for preliminary assessment of the slope FS, the use of LE for more accurate FS estimation and the prediction of critical slip surfaces, and the use of FDM for slope displacement modelling. The analysis incorporates different water table geometries to determine the specific groundwater condition that led to the 2020 landslide by comparing the modelling results with field observations. This research offers further insights into the groundwater control on landslide occurrence and the influences of soil characteristics on landslide development. The findings provide a basis for an improved understanding of the failure mechanisms of colliery spoil tip landslides in Wales, highlight the detrimental effects of increased pore pressures associated with heavy rainfall or future storm events, and emphasise the need for improved water management strategies for the region.

2. Study Area Description

The geometry of the Wattstown tip is a cone-shaped heap, spanning over 85,000 square m. It was created by waste or spoil discarded by the Cwch (National) Colliery, which deposited over 1,000,000 cubic m of colliery spoil on a naturally sloping terrain. In general, the colliery spoils in the Welsh coalfield are comprised of coarse-to-fine colliery discard with weak cohesion [36,37]. The tip is situated approximately 380 m south of a nearby village in the Rhondda Fach Valley that was established as a residential community for miners employed at the Cwch (National) Colliery (Figure 1).

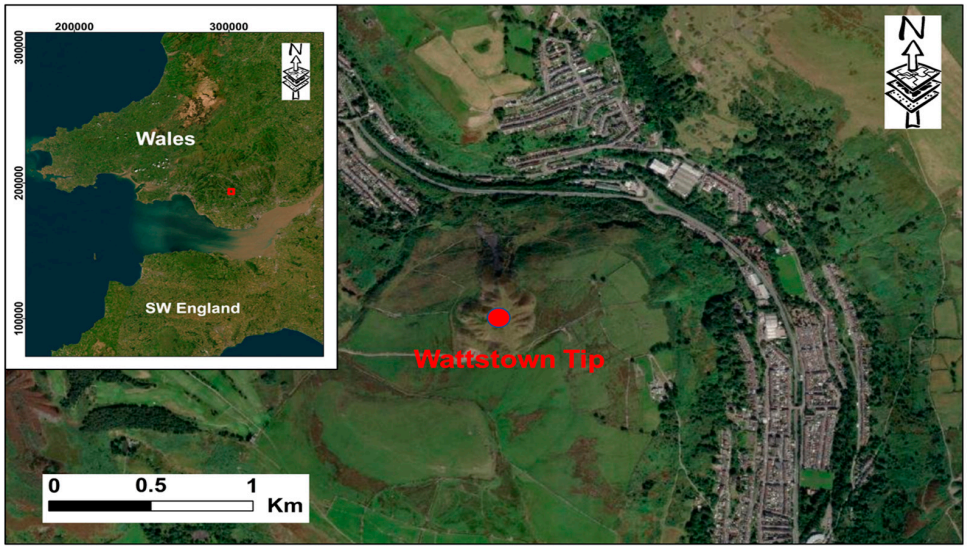

Figure 1. Study area—Wattstown tip which is south of Wattstown in the county borough of Rhondda Cynon Taf, Wales, and displayed on ESRI world imagery.

The natural slope has undergone extensive quarrying of a sandstone unit 12 m in thickness. The unit was characterised by a massive pennant with irregular bands of grey-blue silty mudstone that reached up to 1.8 m in thickness [38]. It was exposed following the sliding of failure material as shown in Figure 2c.

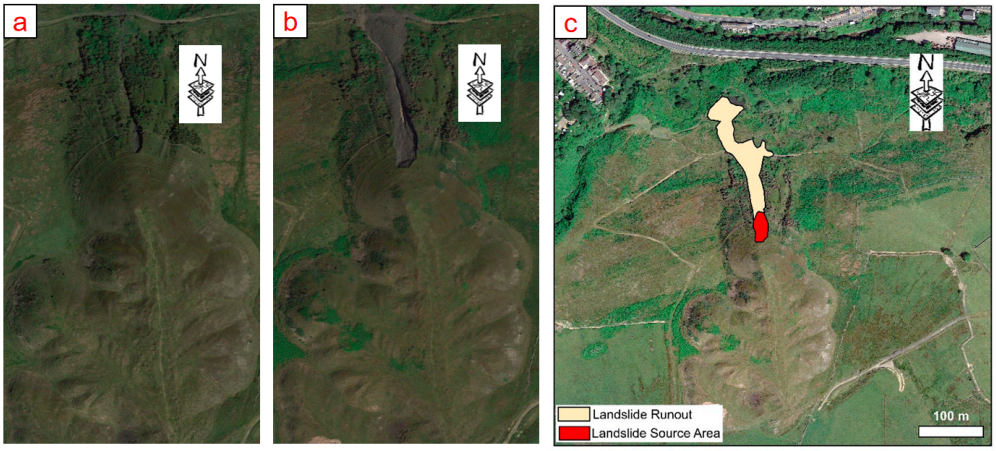

Figure 2. Images of Wattstown standard tip. (**a**) A Google satellite image prior to the landslide (05/2020), (**b**) a Google satellite image after the landslide (07/2021), (**c**) delineation of the landslide boundary.

On 18 December 2020, a landslide event was identified as occurring in a previously established landslide scarp, as can be seen in the comparison between Figure 2a,b. The landslide was recognised as a shallow rotational slide in the slope face. Its extent was

delineated on a Google satellite image, as shown in Figure 2c, highlighting its source area and runout from the south face of the tip. The runout travelled approximately 250 m along a pre-existing trench and spread out from the source area in a fan-like shape, consequently reaching the scrubland at the toe of the slope.

HadUK-Grid provides a daily rainfall data set consisting of 5 km × 5 km grids over the UK [39]. The rainfall data located at the study area indicate that the landslide happened after continuous rainfall which commenced from 9 December 2020 with 20.7 mm and achieved a maximum of 52.8 mm daily rainfall on the day of the landslide (Figure 3).

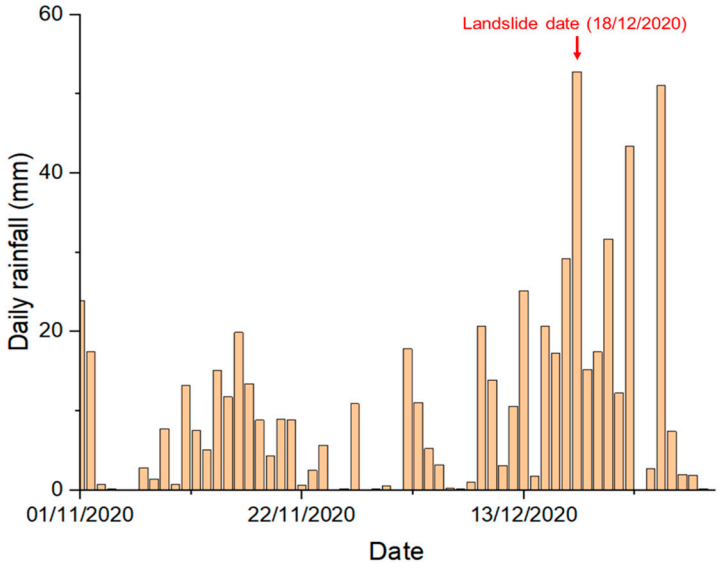

Figure 3. Daily rainfall located at the study area from November 2020 to December 2020 (Met Office Hadley Centre, 2023).

Minor failure scars and distinct water channels were observed on the north face prior to the 2020 landslide (Figure 2a). They are also highlighted by shadows on the hillshade map (Figure 4a) that was used to simulate the effects of the sun's rays on the three-dimensional terrain surface. The hillshade map was created from a 1-m digital terrain model (DTM) (2011) which was acquired from an open-source database, DataMapWales [40]. The existence of water erosion gullies or channels implies poor surface water management and relatively weak or easily eroded material making up the colliery spoil. The north face of the tip was characterised by a 50 m high slope with inclination ranging roughly from 30° to 40°. Both flanks (east and west) were less inclined: approximately 30° in general, as seen in Figure 4b,c.

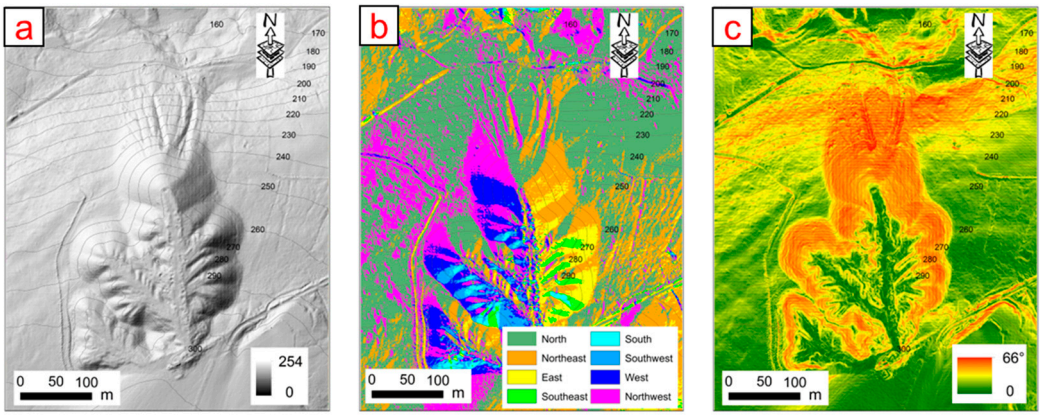

Figure 4. Remote-sensing mapping of the Wattstown standard tip prior to the 2020 landslide occurrence. (**a**) Hillshade map, (**b**) aspect map, and (**c**) slope angle map.

3. Methods of Analysis

Back analysis of previous instability can provide a useful insight into understanding the underlying mechanisms controlling instability and also provide an indication of the likely material properties on specified failure surfaces or groundwater conditions required to trigger initial instability. It is also a useful approach to assess the likely material properties at failure when data such as soil strength properties are limited or scarce. Different methods have been utilised to back-analyse the 2020 landslide, including stability charts, 2D LE analysis, and 3D FDM modelling (Figure 5).

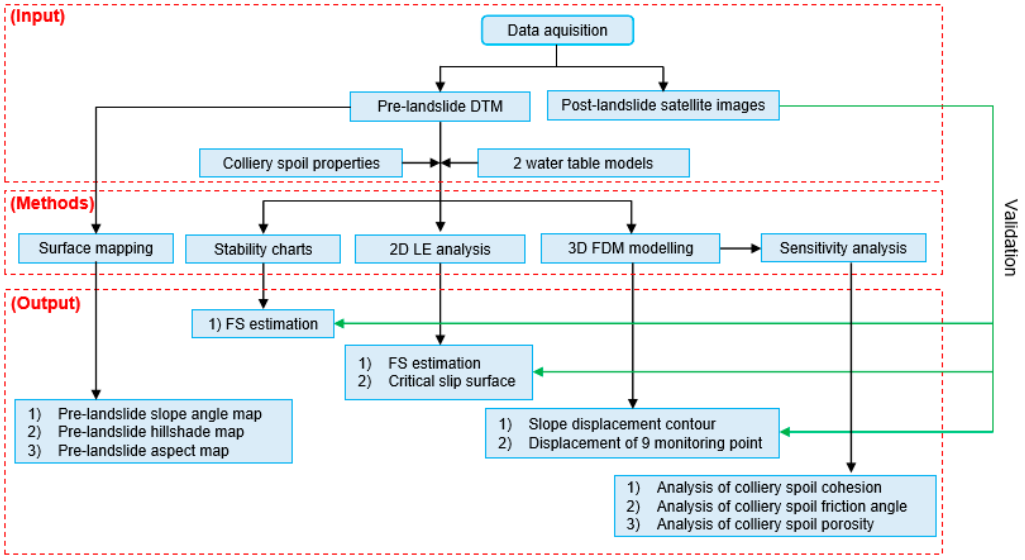

Figure 5. Methodology of this research, including the input part to collect data for landslide analysis, the methods part of different methods used for landslide analysis, the output part of the final results obtained using these methods, and the validation process using post-landslide satellite images.

Given that the landslide occurred after a period of heavy precipitation, back analysis of the failure has been undertaken to assess the impact of varying groundwater tables on tip stability. Varying groundwater table geometries were assessed within the numerical modelling (LE and FDM modelling). In addition, sensitivity analyses were also conducted to assess the influence of the variation in both soil properties and groundwater levels on tip stability.

3.1. Investigation of Tip Properties

Table 1 provides the typical colliery spoil properties assumed for the analysis, including the unit weight (γ), friction angle (ϕ), cohesion (c), and porosity (φ). This was supported with data obtained from the relevant literature. However, these properties exhibit significant variability from site to site and are highly dependent on the on-site climate, topography, geology, vegetation, and human activities.

Table 1. Colliery spoil properties characterised by their variations from minimum to maximum values with the summary of references.

Soil Property	Mean	Minimum	Maximum	Reference
Unit weight (KN/m^3)	19	17	21	[37,41–46]
Friction angle (°)	37	32	42	
Cohesion (KPa)	10	0	20	
Porosity (%)	20	10	30	

Prior to analysis, two slope models (2D and 3D) were created using the 2011 LiDAR DTM data to depict the pre-landslide tip geometry, as presented in Figure 6. The 3D model

was developed through extrusion of the DTM to the base plane of 150 m above the ordnance datum (Figure 6a). Several points were placed on the surface of the model to monitor the surface slope displacement in FDM modelling (Figure 6b). The 2D model (cross section) was generated along an N–S profile that intersects the points P7–P6–P1–P8–P9 (Figure 6c).

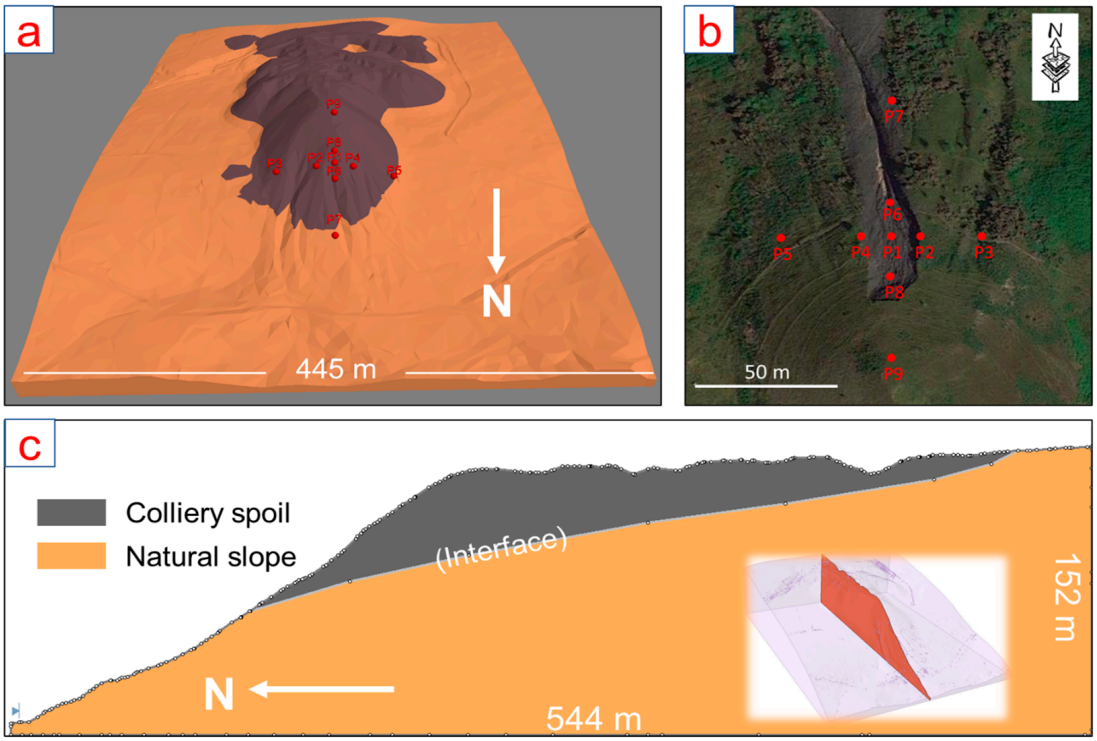

Figure 6. Slope models for numerical analysis. (**a**) A 3D model and 9 monitoring points, (**b**) a satellite image showing the position of the 9 points, (**c**) a 2D model constructed along an N–S profile in the 3D model.

3.2. Circular Failure Charts

Various stability chart solutions are available to estimate the FS of soil slopes. Considering their assumptions and limitations, the approach proposed by Hoek and Bray [24] was utilised to determine the FS. This approach consists of a set of 5 circular failure charts, providing a rapid check on the FS of a slope, or upon the sensitivity of FS to the change in the groundwater conditions, slope angle, and material strength properties. Figure 7 shows a representative chart to assess the slope stability where the surface water is 8×H behind the toe of the slope.

The primary assumptions for Hoek and Bray stability charts include the following:

(1) The material forming the slope is homogeneous;
(2) The shear strength (τ) of the material is defined by the cohesion (c) and friction angle (Φ);
(3) The potential circular slip surface passes through the toe of the slope.

Mean values of the soil properties were employed (Table 1). The key soil parameters in the charts include the unit weight of soil ($\gamma = 19$ KN/m^3), the height of the slope (H = 50 m), the soil friction angle ($\Phi = 37°$), and the soil cohesion (c = 10 kPa). In addition, the analysis also accounts for the potential impact of the variation in the slope inclination of the north face by considering different slope angles ranging from minimum (30°) to maximum (40°), thus encompassing all possibilities associated with the stability results.

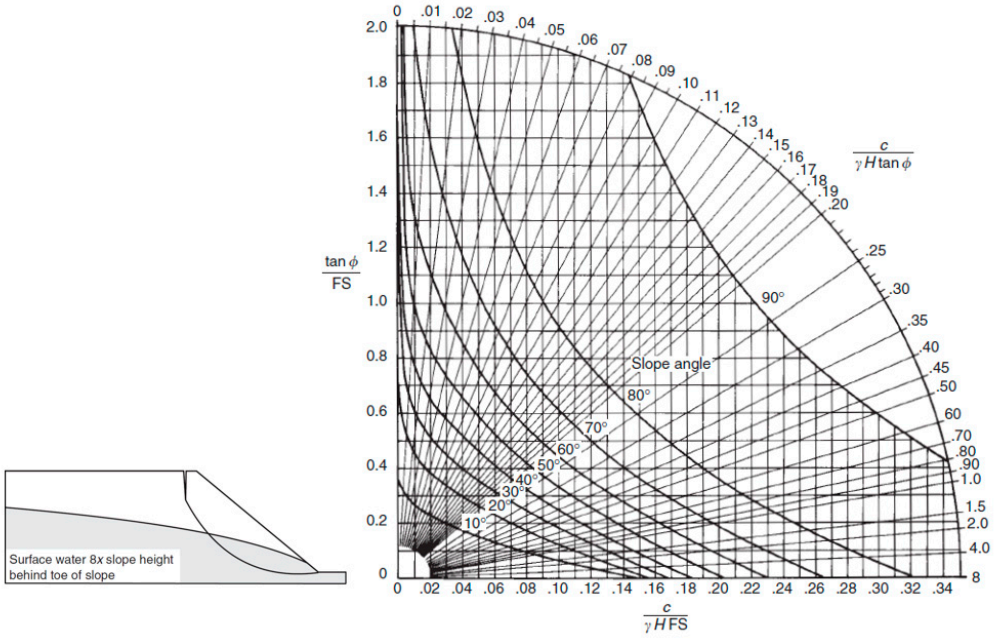

Figure 7. A representative Hoek and Bray circular failure chart to estimate the FS of a soil slope where the surface water is 8×H behind the toe of the slope.

3.3. Three-Dimensional Limit Equilibrium Analysis

In this study, Slide2 (version 9.034), developed by Rocscience Inc. (Toronto, ON, Canada) [47], was used for limit equilibrium analysis. The modelling takes into account the slope geometry, heterogeneous slope materials, and varying groundwater conditions. The programme is widely used by geotechnical engineers and researchers for analysing the stability of soil and rock slopes, designing safe slopes, and evaluating the risk of slope failures at a low computational cost [48–50]. The analysis incorporates different LE solutions, such as the simplified Bishop method [26] and simplified Janbu method [51], as well as the Spencer method [27], to compute the FS of critical slip surfaces.

Observations suggest that the 2020 landslide was a shallow rotational failure within the layer of colliery material. Between the colliery spoil and the underlying natural slope, a geological interface was created to act as a material boundary in LE analysis. In LE analysis, the soil mechanical behaviour was constrained by the Mohr–Coulomb failure criterion, expressed as

$$\tau = c + \sigma tan\Phi \quad (1)$$

where τ is the shear strength, c is the soil cohesion, σ is the normal stress, Φ is the friction angle. The material properties for the model (the colliery spoil and natural slope) adopted in this research are presented in Table 2.

Table 2. Soil properties for the colliery tip and underlying natural slope for LE numerical analysis.

	Friction Angle	Cohesion	Tensile Strength	Porosity
Colliery tip	37°	1×10^4 Pa	0	20%
Natural slope	40°	1×10^5 Pa	5×10^4 Pa	10%

Back analysis was performed to explore the groundwater condition of the landslide accident. This was achieved by establishing a range of water tables in the modelling and searching for the one contributing to a limit equilibrium state of the recreated landslide profile.

3.4. Three-Dimensional Finite-Difference Method

A 3D FDM method was employed to analyse the landslide development in a real scenario of 3D slope geometry. This was carried out by utilising FLAC3D 6.0 [52] and incorporating heterogeneous slope materials. The code uses an explicit time-stepping solution to solve equations of motion, simulating the mechanical response of soils that are subject to either static or dynamic loading. Additionally, It is capable of modelling fluid through porous media using its built-in Fluid Grid Model, such as groundwater flow through soil. Thus, the code has been widely used in the field of slope stability analysis [53–55].

In FDM modelling, soil behaviour was constrained by the Mohr–Coulomb failure criterion. The key parameters that define the Mohr–Coulomb failure criterion are summarised in Table 3, including the friction angle (Φ), cohesion (c), tensile strength (σ), elastic bulk modulus (K), and elastic shear modulus (G). The values of the strength properties (i.e., Φ, c, and σ) used here were identical to those used in the LE analysis.

Table 3. Strength and deformability properties of colliery spoil and natural slope used for FDM modelling.

	Friction Angle	Cohesion	Tensile Strength	Bulk Modulus	Shear Modulus
Colliery spoil	37°	1×10^4 Pa	0	1.67×10^8 Pa	0.77×10^8 Pa
Natural slope	40°	1×10^5 Pa	5×10^4 Pa	8.33×10^8 Pa	4×10^8 Pa

A set of 3D water table geometries were created to characterise the 3D representation of the hydrogeological conditions corresponding to the dry and partially saturated slope. The pore water pressure (u) below the water table is calculated as follows,

$$u = g_w \times h \quad (2)$$

where g_w is the unit weight of water; h is the depth below the water table. The pore water pressure above the water table is 0. This became a boundary condition applied in FDM modelling. Boundaries were extended from the zone of interest to ensure no boundary effects. A fixed boundary condition was applied to the sidewalls and the base. To monitor slope displacement along with modelling timestep, 9 points were placed in the model as shown in Figure 6. Only P7 was located in the natural slope material, with the remaining points placed in the colliery spoil.

3.5. Sensitivity Analysis

The properties of colliery spoil exhibit variation across different locations. In addition, soil properties can be affected by the presence of water in the voids between soil particles [56,57], implying that they have the potential to undergo alterations during precipitation events. To evaluate the potential impact of soil variations on slope behaviour, sensitivity analysis was performed concentrating on critical colliery spoil properties, such as cohesion, friction angle, and porosity. Variations in these parameters were represented by the mean value, minimum and maximum, as shown in Table 1. For each analysed parameter, a sensitivity analysis was conducted by varying its value from the minimum to the maximum and analysing the effect of this change.

4. Results

4.1. Results of Stability Chart Analysis

Figure 8 summarises the results of stability chart analysis associated with different groundwater conditions. The figure reveals that a slope with a lower inclination obtains a relatively high FS in an analogous groundwater condition. Furthermore, all the FS lines exhibit a declining trend with an increase in water table, which is a common phenomenon induced by additional pore water pressure. The FS undergoes a sudden reduction from the

8×H groundwater condition to the 2×H groundwater condition, ultimately approaching values that are less than 1.

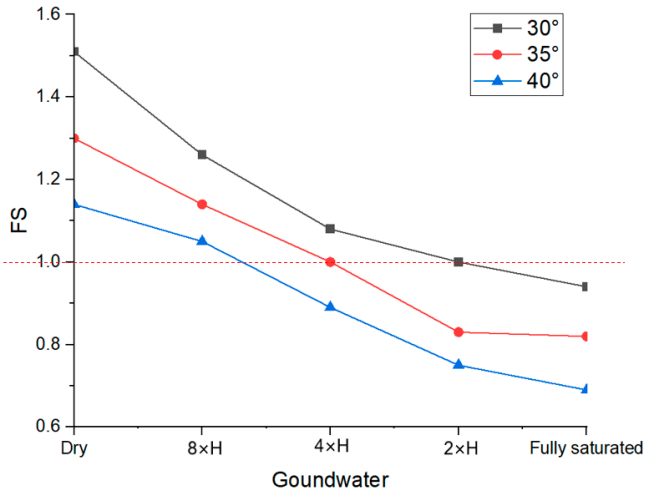

Figure 8. FS values of the slope angle of 30° (grey line), 35° (red line), and 40° (blue line) in response to different groundwater conditions.

For a slope angle of 30°, the FS is estimated to be 1.5 when the slope is dry, indicating a stable state. It decreases to approximately 1 at the 2×H condition; For a slope angle of 35°, the initial FS of 1.3 suggests a relatively stable slope in the dry condition, but it decreases to 1 at the 4×H groundwater condition. For the slope angle of 40°, the dry slope is evaluated as a stable state as the FS is close to 1.13, but the FS drops to 0.9 at the 4×H groundwater condition.

4.2. Results of Numerical LE Analysis

Figure 9 presents the outcomes of the representative LE analysis using the simplified Bishop method, showing the recreated slip surface and associated FS values. When the slope is dry, the FS of the failure zone is approximately 1.471 (Figure 9a), which means the slope is considerably stable and the rational landslide would not happen in such a water condition. However, as the water table increases to regime_1 (Figure 9b), the FS decreases to 1 when the slope and failure zone is partially saturated. At this limit equilibrium state, the critical water table intersects the failure zone and provides the pore water pressure to drive the rotational landslide.

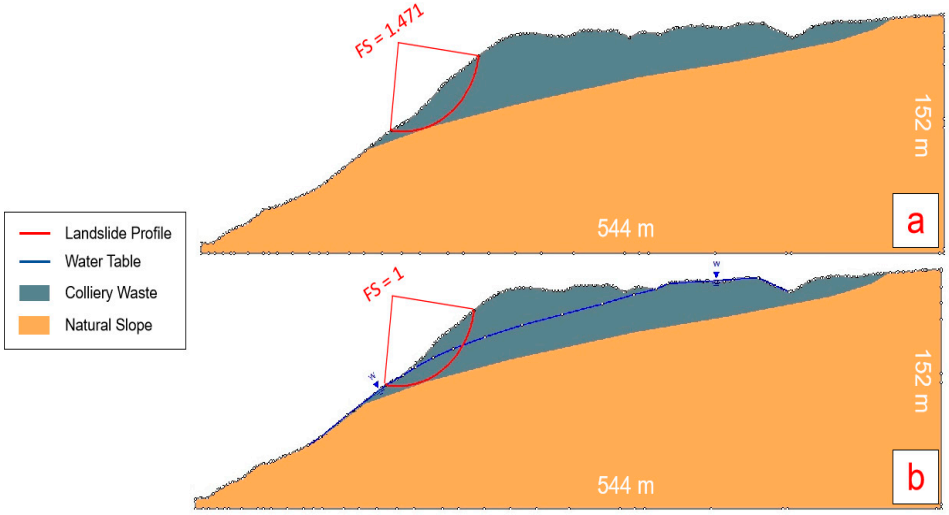

Figure 9. Results of 2D LE analysis based on the simplified Bishop method, showing FS estimation corresponding to the slip surface. (**a**) Dry slope, (**b**) partially saturated slope (regime_1).

Table 4 summarises the FS values estimated by using different methods. Similar results were obtained from simplified Bishop and Spencer analysis. They both indicate a limit equilibrium state of the failure zone once the water table reaches regime_1. However, a lower estimation of the FS was produced by simplified Janbu compared with the other two methods.

Table 4. FS estimation in various hydrogeological conditions by using different LE methods, including the simplified Bishop method, simplified Janbu method, and Spencer method.

Method	Dry Slope	Partially Saturated Slope (Regime_1)
Simplified Bishop	1.471	1
Simplified Janbu	1.28	0.897
Spencer	1.464	1.019

4.3. Results of 3D FEM Modelling

All FDM simulations reached a conclusion at the 10,000 timestep for comparison and to understand the influence of the groundwater conditions on the slope stability.

4.3.1. Dry Slope

The modelled total displacement contour for a dry slope is presented in Figure 10. The slope achieves the maximum total displacement of approximately 0.5 m in the colliery spoil in the north face. An N–S cross section was taken through the central section of the model to inspect the total displacement in the model, and only minor total displacement was observed. In addition, the displacement curves in Figure 11 reveal that the nine points converge to constant values. These results indicate that the slope is stable under a dry condition.

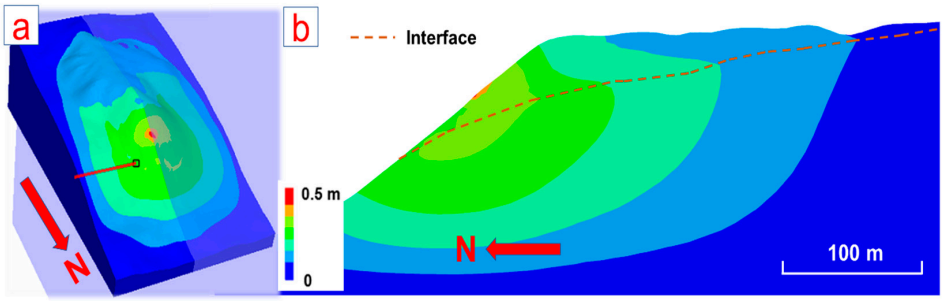

Figure 10. FDM modelling result showing the total displacement of a dry slope (regime_1). (**a**) overview of the modelling result, (**b**) an N–S cross section of the total displacement contour.

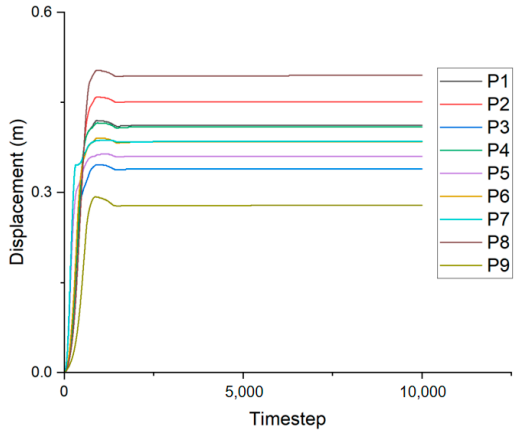

Figure 11. The curves of total displacement at 9 monitoring points when the slope is in a dry condition.

4.3.2. Partially Saturated Slope

Figure 12 depicts the modelled total displacement contour when the slope is at the regime_1 water level. The modelling shows a distinct variation in soil displacement that is located in the failure zone (Figure 2). The maximum total displacement of approximately 3 m is observed in the north face, while negligible low values are observed on the other sides. The N–S cross section indicates that the modelled unstable zone is spatially constrained by the underlying interface (between natural slope and colliery spoil) and overlying water table, and it is characterised by a shallow translational failure (see Figure 12b). The displacement vectors in Figure 12a indicate that the failure body moves downslope towards N. Figure 13 presents the curves for total displacement monitored at the nine points in the regime_1 condition. The centre point (P1) has the highest displacement. P4 and P6 are displaced more than P2 and P8. The displacement of points P3, P5, P7, and P9, which are located outside the central zone showing the displacement vector, converge at 0.7 m.

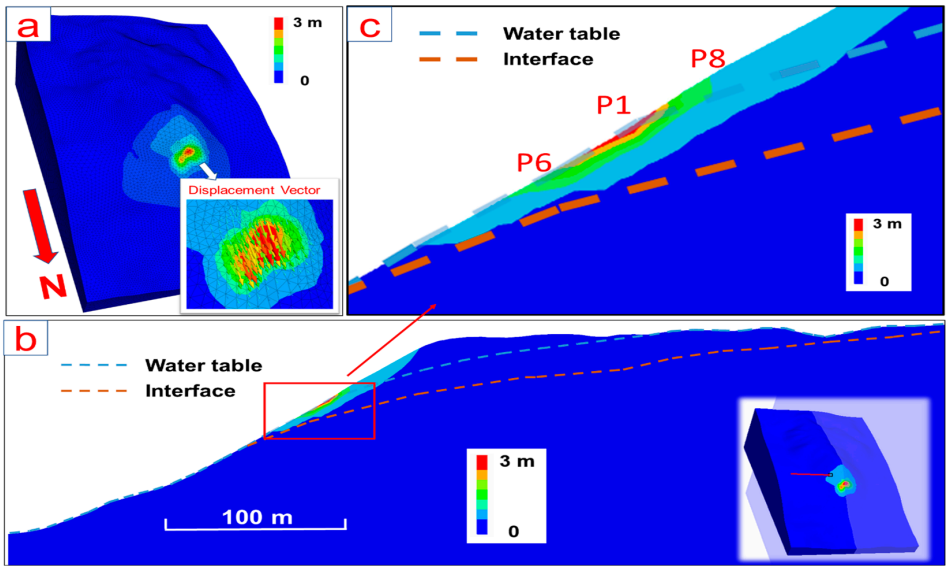

Figure 12. FDM modelling result of a partially saturated slope (regime_1). (**a**) Contour of slope displacement and modelled displacement vectors of the unstable zone, (**b**) an N–S cross section of the slope displacement contour, (**c**) close-up image of the N–S cross section showing the geometry of the unstable zone and monitoring points P1, P6, and P8 on the slope.

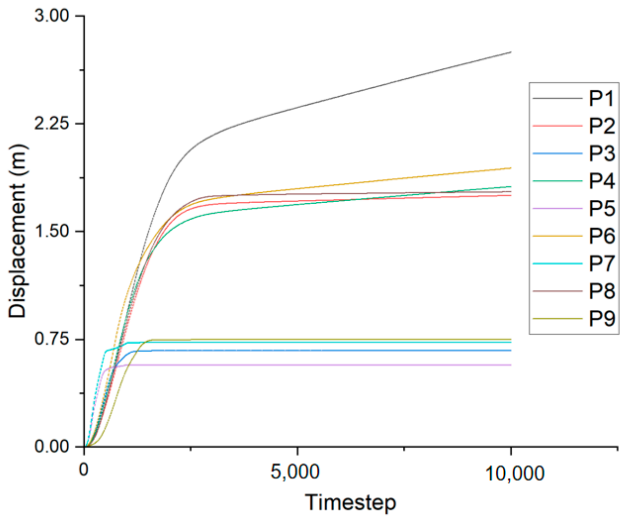

Figure 13. The curves of total displacement at 9 monitoring points when the slope is in the regime_1 water condition.

4.4. Result of Sensitivity Analysis for Colliery Spoil Properties

4.4.1. Sensitivity Analysis of Soil Cohesion

The modelled unstable zone highlighted in Figures 9b and 12 is consistent with the field observations (Figure 2) which infers that the Wattstown landslide is the result of changes in pore pressure associated with a rise in the water table following heavy rainfall. In this context, a further sensitivity analysis was performed to assess the impact of variations in tip material properties and is defined by a 3D representation of the regime_1 groundwater condition.

Figures 14 and 15 show the results of sensitivity analysis associated with the variation in the cohesion of colliery spoil that ranges from a minimum of 0 to a maximum of 20 kPa. The total displacement curves of monitored points indicate that increased model displacement occurs when the tip is composed of cohesionless colliery material (Figure 14a) when compared to a slope material that has the mean cohesion value (Figure 13). In particular, P2 exhibits an exponential rise in displacement with the decrease in cohesion to 0. In addition, P3 becomes unstable, which is characterised by a continuous rise in displacement in Figure 14a. Once the cohesion increases to 20 kPa, the slope converts to a stable state in the modelling. The displacement curves of all monitored points achieve convergence, as seen in Figure 14b. In addition, no differential displacements are observed in the modelling following the initial equilibrium condition (Figure 15b,d).

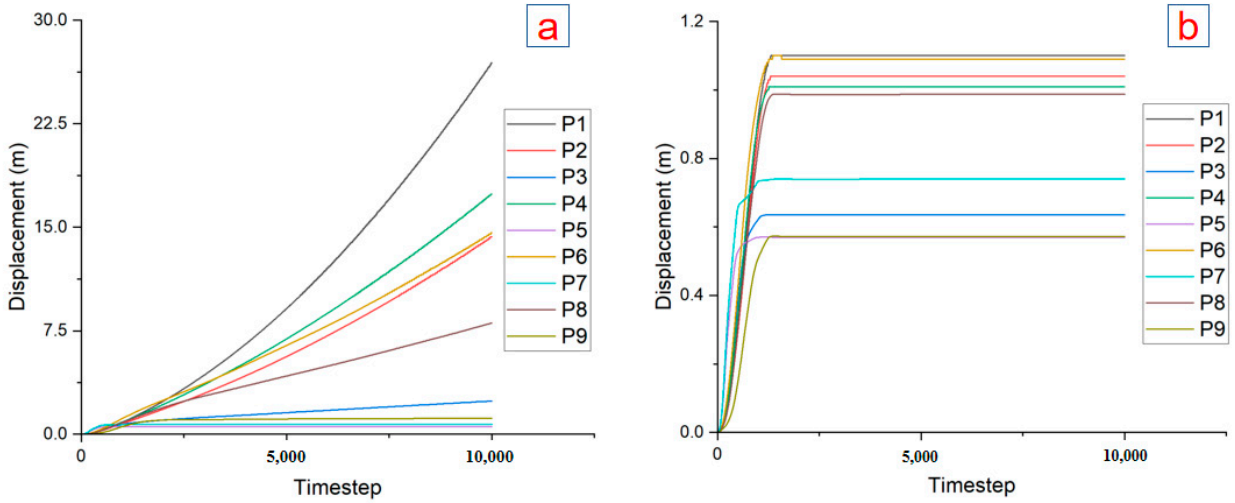

Figure 14. The curves of total displacement at 9 monitoring points. (**a**) c = 0, (**b**) c = 20 kPa.

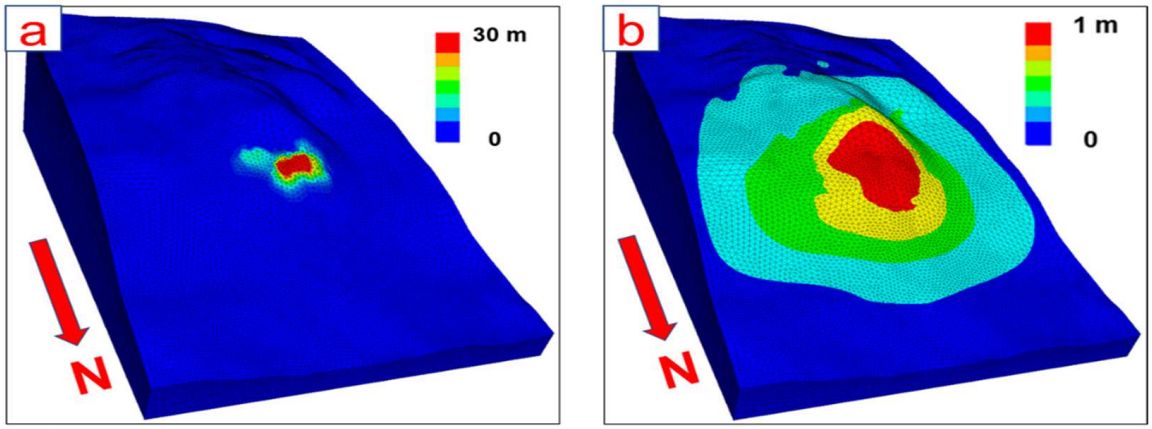

Figure 15. *Cont.*

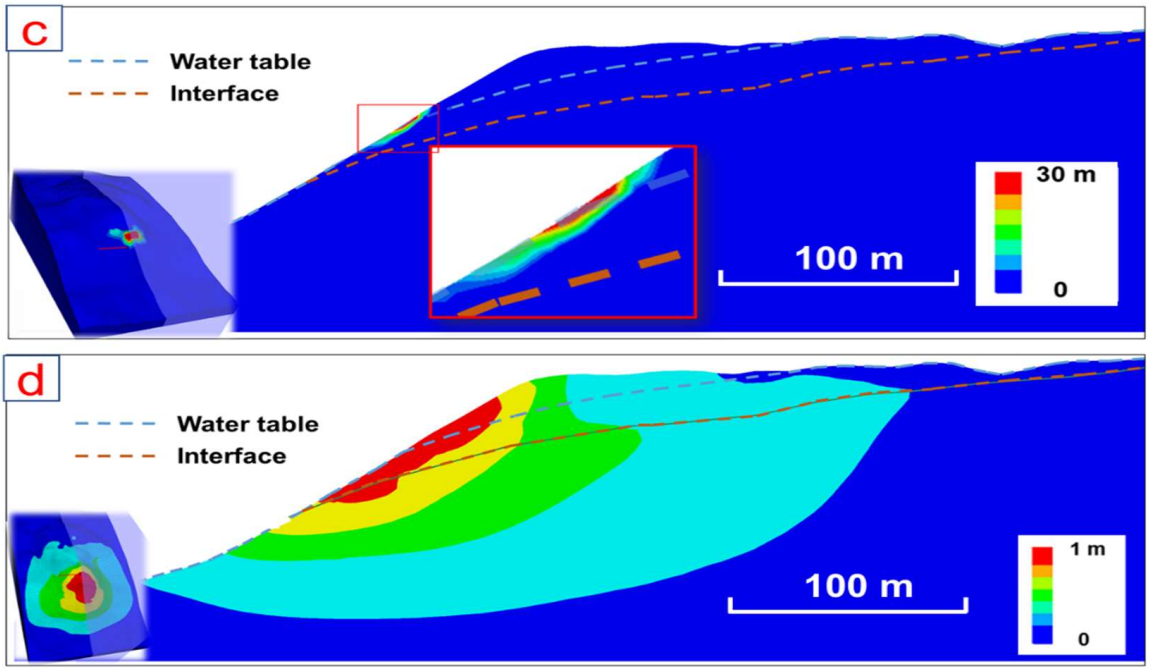

Figure 15. Results of sensitivity analysis associated with the cohesion of colliery spoil. (**a**) c = 0, (**b**) c = 20 kPa, (**c**) N–S cross section of the cohesionless modelling result, (**d**) N–S cross section of the 20 kPa modelling result.

4.4.2. Sensitivity Analysis of Soil Friction Angle

Figures 16 and 17 present the results of sensitivity analysis associated with the variation in the friction angle of colliery spoil that ranges from a minimum of 32° to a of maximum 42°. The points (P3, P5, P7, and P9) remain stable when the friction angle decreases from 37° to 32° as seen in Figure 16a. In addition, the unstable zone is also constrained by the water table and the natural ground interface (Figure 17a,c). However, the model that has a decrease in the friction angle results in additional displacements of the points (i.e., P1, P2, P4, P6, and P8), which is more obvious for P2 and P8 that become unstable in the modelling.

When the friction angle is 42°, the slope becomes stable. The total displacement curves of all monitored points achieve convergence as seen in Figure 16b. In addition, no differential displacements are observed in the modelling following the initial equilibrium condition (Figure 17b,d).

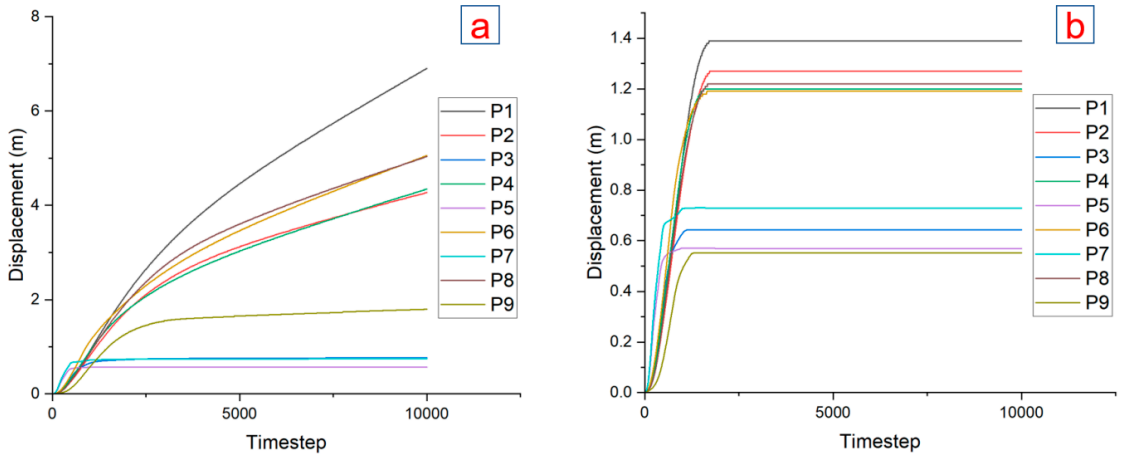

Figure 16. The curves of total displacement at 9 monitoring points. (**a**) Φ = 32°, (**b**) Φ = 42°.

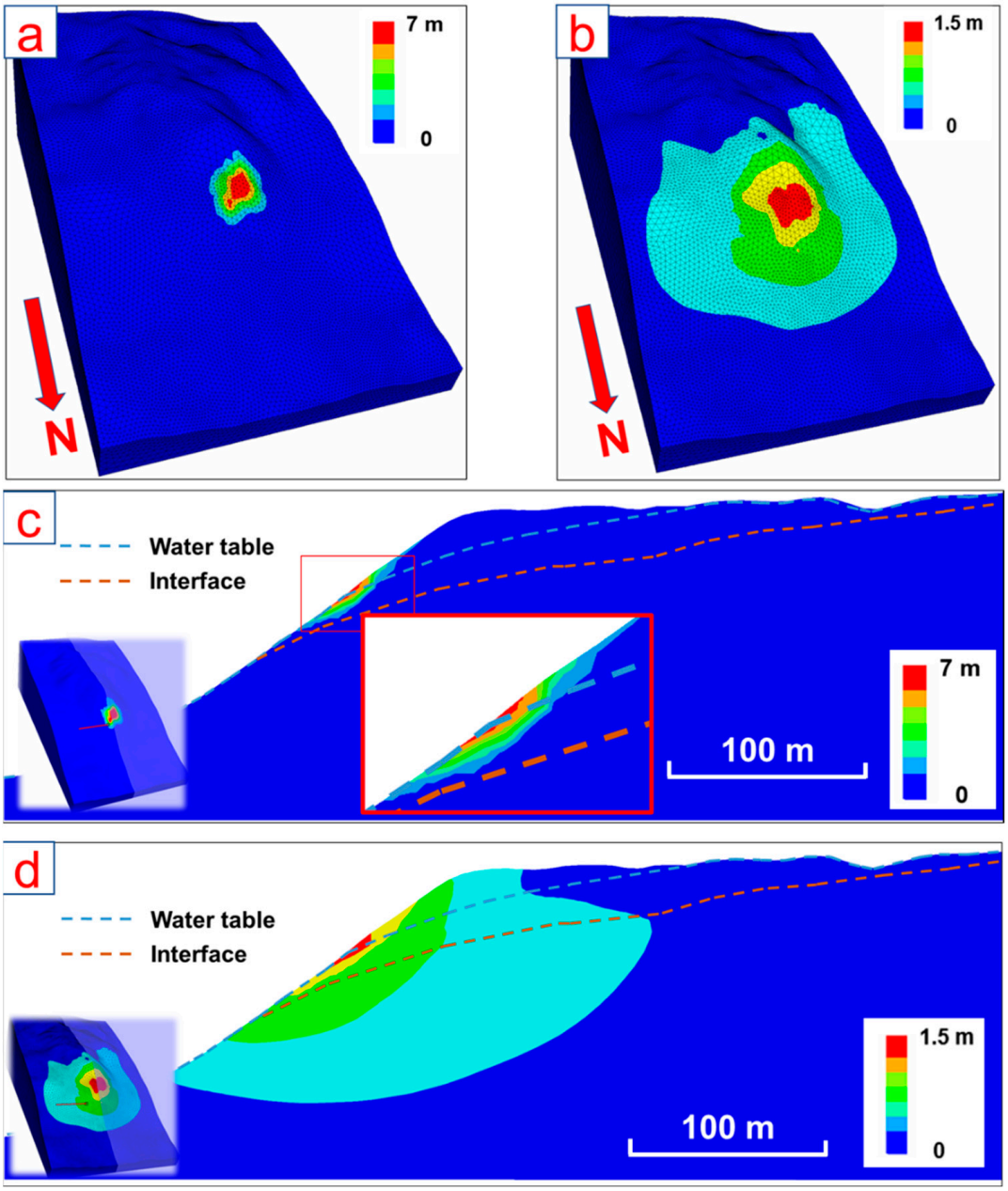

Figure 17. Results of sensitivity analysis associated with the friction angle of colliery spoil. (**a**) Φ = 32°, (**b**) Φ = 42°, (**c**) N–S cross section of the 32° friction angle modelling result, (**d**) N–S cross section of the 42° friction angle modelling result.

4.4.3. Sensitivity Analysis of Soil Porosity

Figures 18 and 19 exhibit the results of sensitivity analysis related to the variation in the porosity of the colliery material that ranges from a minimum of 10% to a maximum of 30%. Similar to the modelling result of the mean porosity (Figure 4), the points (P3, P5, P7, and P9) remain stable when the porosity is 10% as seen in Figure 9a. In addition, the unstable zone is also constrained by the water table and the interface (Figure 19a,c). More displacements of the points (i.e., P1, P2, P4, P6, and P8) are identified with the decrease in porosity. P2 and P8 exhibit a trend of linear increase in the total displacement as well. When the porosity raises to 30%, the entire slope becomes stable with a maximum total displacement of approximately 2 m (Figure 19b,d).

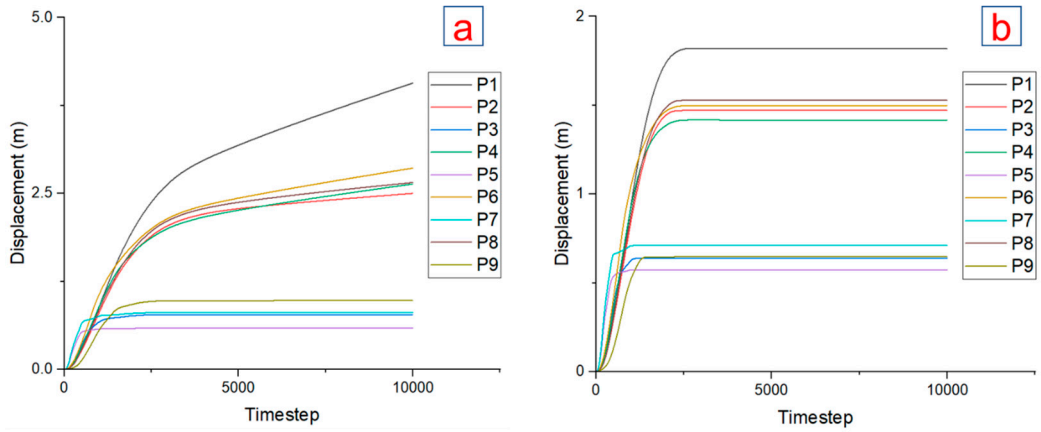

Figure 18. The curves of total displacement at 9 monitoring points. (**a**) φ = 10%, (**b**) φ = 30%.

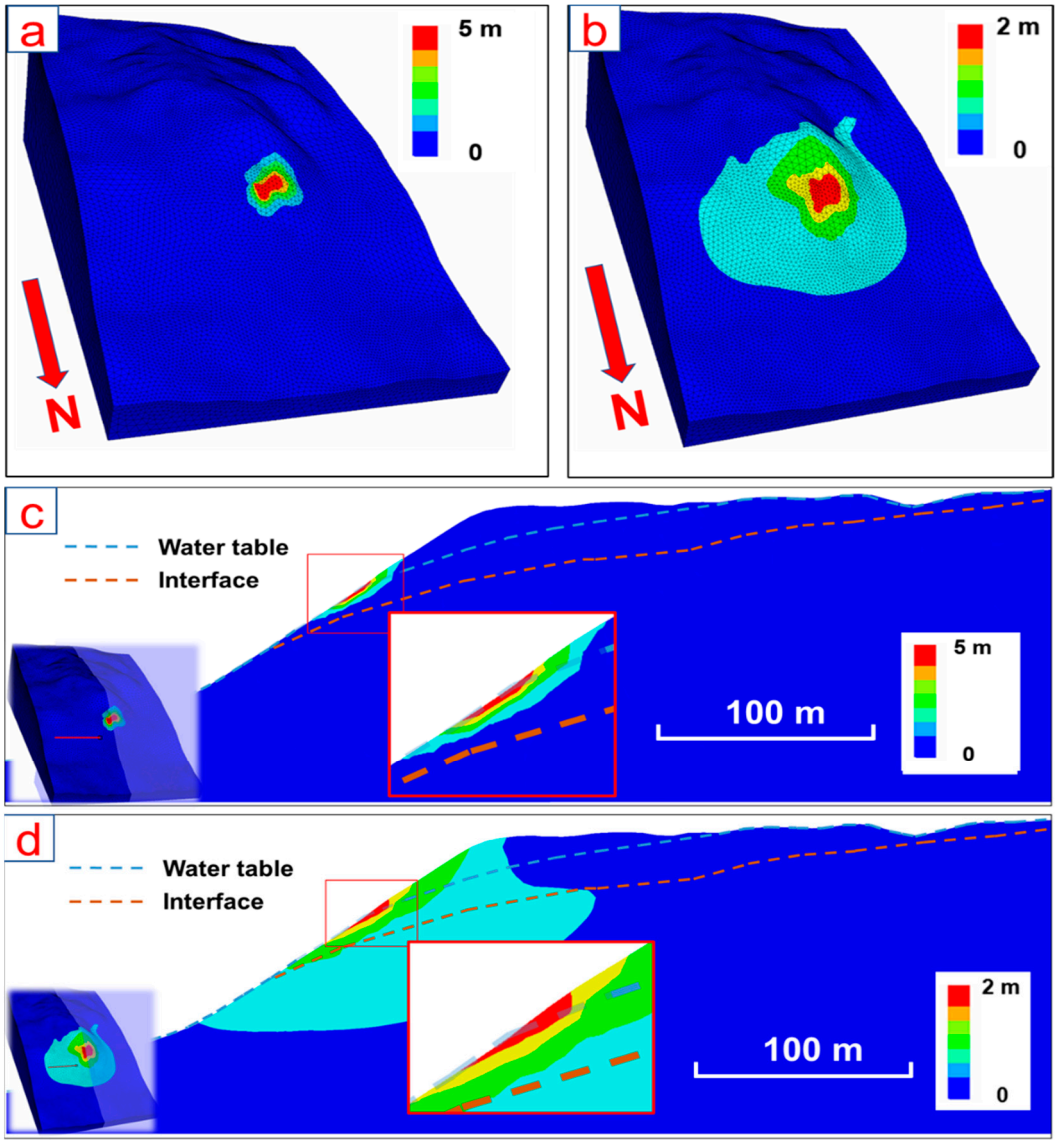

Figure 19. Results of sensitivity analysis associated with the porosity of colliery spoil. (**a**) φ = 10%, (**b**) φ = 30%, (**c**) N–S cross section of the 10% porosity modelling result, (**d**) N–S cross section of the 30% porosity modelling result.

5. Discussion

Previous research has highlighted that slopes with materials that have a low cohesion (e.g., 10 kPa cohesion of colliery spoil in this research) and tensile strength and are sensitive to groundwater variation and thus to the change in groundwater regime [58–60]. This is also reflected in the sensitivity analyses undertaken as part of this research, through numerical stability analysis on different groundwater regimes. The slope is evaluated as stable in a dry condition (Figures 9, 10a, 11 and 12), which infers that the soil shear strength is competent to resist the gravity-induced driving force. In the regime_1 groundwater condition where the water table overlies the geological interface, the slope is prone to face failure (Figures 10b and 15). The modelled failure occurred in the colliery spoil layer and was constrained by the water table and the underlying geological interface. The location and size of the unstable zone in the modelling is consistent with field observations (Figure 2) for the Wattstown tip failure. These results together indicate that the Wattstown tip landslide may have occurred when the slope was partially saturated (i.e., with the water table above the natural slope but below the slope geometry).

Both 2D LE analysis and 3D FDM analysis produced consistent results in terms of the slip surface estimation under different groundwater conditions. However, the main difference between the two methods lies in the computational time required. Two-dimensional LE analysis can be completed very quickly (order of minutes), while each 3D FDM simulation can take several hours (depending on the computing hardware). Despite the fact that the 2D LE analysis did not consider certain aspects, such as the 3D slope topography and soil displacement, the similarity of the results between the 2D LE analysis and the more comprehensive 3D FDM modelling suggests that the former could serve as an indicator for rapid and preliminary estimation of soil slope stability. This approach could be particularly useful in Wales, where a significant number (327) of tips have been identified as having high potential safety risks.

Sensitivity analyses have identified the impact of key soil properties on slope stability. It is found that the stability analysis of the Wattstown colliery tip is very sensitive to soil strength. For example, variations in soil cohesion from 0 to 20 kPa can lead to totally different slope stability conditions and also soil displacement behaviours.

Monitoring of the rainfall duration, intensity, and likelihood of occurrence is necessary to predict potential instability. Continuous monitoring of the rainfall can provide an early warning of potential slope failures, allowing for the timely evacuation of people and property in high-risk areas. The UKCP18 project, which is part of the UK Met Office Hadley Centre Climate Programme, produced climate change projections up to the year 2100 in the UK using previous observation data [61]. The data for projected daily precipitation provide a potential reference to assess rainfall-induced landslide events for areas such as Welsh coalfields [62]. For example, Figure 20 shows the anticipated daily precipitation projection for a 5 km grid located in the Wattstown study area from 1 July 2024 to 31 December 2028. Previous studies suggested that both extreme single-day precipitation and accumulative precipitation can trigger landslides [63,64]. In this context, Table 5 records the number of events that predicted daily precipitation exceeding specific thresholds. In addition, Table 6 summarises the number of events that the amount of three-day accumulative precipitation exceeds specific thresholds and simultaneously the single-day precipitation exceeds 10 mm. The data indicate that most of these predicted extreme precipitation events occur in winter.

Table 5. The number of events that the amount of single-day precipitation exceeds specific thresholds from 1 July 2024 to 31 December 2028.

	2024	**2025**	**2026**	**2027**	**2028**
50–60 mm	1	2	3	3	1
60–70 mm	1	1	1	0	1
≥70 mm	1	1	0	0	1

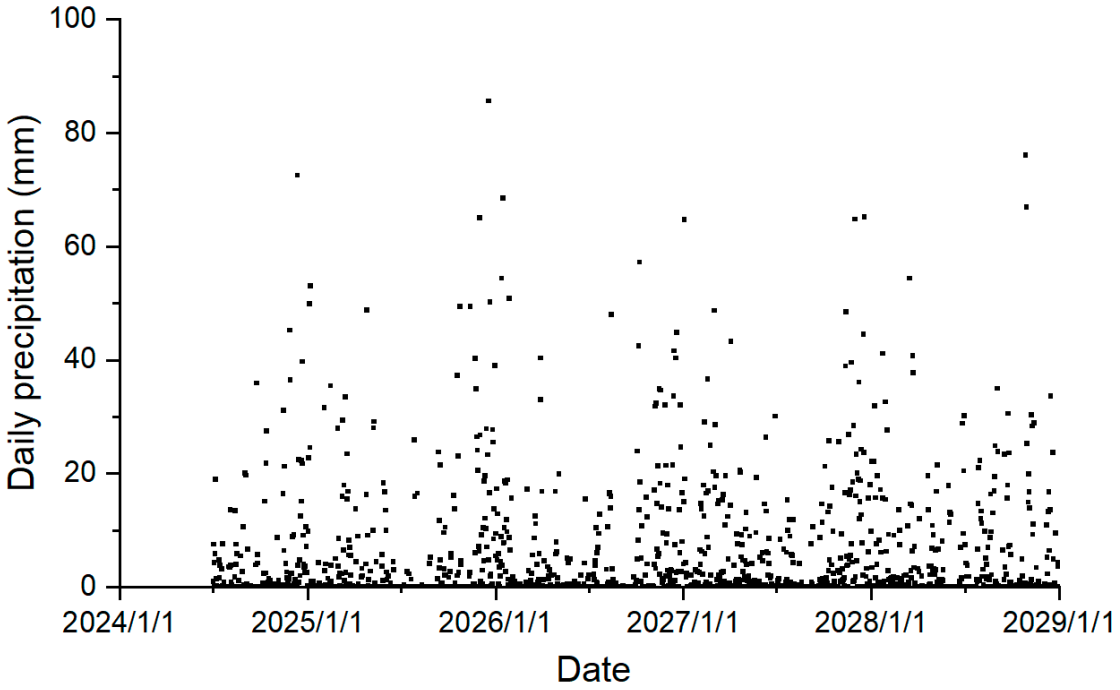

Figure 20. UKCP18 daily precipitation projection of a 5 km grid located in the study area from 1 July 2024 to 31 December 2028.

Table 6. The number of events that the amount of three-day accumulative precipitation exceeds specific thresholds from 1 July 2024 to 31 December 2028.

	2024	2025	2026	2027	2028
100–115 mm	0	0	1	2	1
115–130 mm	0	1	0	0	0
≥130 mm	0	0	0	1	0

Previous studies have revealed that precipitation and water infiltration can influence the strength and deposition status (e.g., porosity) of unsaturated soils [56,57,65,66]. Further research is required to assess the consequences of dynamic analysis of the mechanical behaviour of unsaturated soils in response to different conditions of precipitation. The understanding of the potential variability of soil suction and soil strength (e.g., cohesion) during precipitation can provide further insight into the mechanism and development of slope instability.

Attention should be drawn to the safety of these colliery spoils in Wales. To prevent similar landslide events in the region, slope stabilisation measures should be taken in time. Considering the key role of groundwater conditions in controlling the slope stability as identified by stability chart analysis (Figure 8), LE analysis (Figure 9), and FDM modelling (Figures 10 and 12), improved surface water management or the reprofiling of tips should be undertaken to minimise instability risks for colliery spoils. As such, drainage is a potential economical and efficient measure to divert water away from spoil tips and reduce the water table in wet seasons. In addition, the revegetation of disturbed land, such as the water erosion channels displayed in Figure 2a, is able to mitigate water infiltration into the slope.

6. Conclusions

This research has investigated the mechanism of the 2020 Wattstown tip landslide through remote-sensing mapping, Hoek and Bray stability chart analysis, 2D LE analysis, and 3D FDM modelling. Different water table geometries were incorporated into these

analyses to identify the groundwater regime that triggered the landslide. In addition, sensitivity analyses of the colliery spoil properties were carried out to estimate the influence of the soil properties on the slope stability analysis. This research provides an improved understanding of the control of groundwater regimes on the development of the landslide. Several conclusions can be made, including the following:

(1) The 2020 Wattstown tip landslide was characterised by a shallow rotational failure mode. It occurred in the steepest north face of the tip with the mean inclination of 35°, travelling along a pre-existing trench and spreading out from the source area in a fan-like shape;
(2) Three-dimensional FDM modelling is capable of recreating the landslide and identifying its source area in the north face. The modelling result was validated by field observation and satellite remote-sensing data post event;
(3) Three-dimensional FDM modelling confirms that the rise of the water table following heavy rainfall most likely triggered the landslide;
(4) The modelling results highlight that the landslide was spatially constrained by the critical water table and an underlying geological interface;
(5) The study demonstrates that as a preliminary investigation tool, both the stability chart analysis and 2D LE analysis are able to effectively predict the slope stability condition of the Wattstown tip. Good consistency was observed between the preliminary investigation and the more sophisticated 3D FDM modelling.

The stability of the colliery tip was assessed using static analysis, assuming that the mechanical and physical properties of soil remain unchanged. This approach may lead to inaccurate modelling of soil behaviours under varying water conditions. Advanced research into the potential variability of soil properties during precipitation is essential to explore the development of colliery tip failure in greater depth in Wales.

Author Contributions: Conceptualisation, L.H., J.C., M.E.; methodology, L.H., J.C., P.F.; software, L.H., J.C., T.P.; validation, L.H., J.C., M.E.; formal analysis, L.H., J.C.; investigation, L.H., M.E.; resources, L.H.; data curation, L.H., T.P., P.F.; writing—original draft preparation, L.H.; writing—review and editing, J.C., M.E.; visualisation, L.H., J.C.; supervision, J.C., M.E. All authors have read and agreed to the published version of the manuscript.

Funding: This research received no external funding.

Data Availability Statement: The raw data supporting the conclusions of this article will be made available by the authors on request.

Conflicts of Interest: The authors declare no conflicts of interest.

References

1. Richards, I.G.; Palmer, J.P.; Barratt, P.A. *The Reclamation of Former Coal Mines and Steelworks*; Elsevier: New York, NY, USA; Amsterdam, The Netherlands, 1993.
2. Welsh Government. Coal Tip Safety | GOV.WALES. Available online: https://www.gov.wales/coal-tip-safety (accessed on 24 March 2023).
3. Siddle, H.J.; Wright, M.D.; Hutchinson, J.N. Rapid Failures of Colliery Spoil Heaps in the South Wales Coalfield. *Q. J. Eng. Geol. Hydrogeol.* **1996**, *29*, 103–132. [CrossRef]
4. Lee, R.G. Disused Coal Tip Management in Wales: Environmental Regulation under Climate Change. *Environ. Law Rev.* **2023**, *25*, 135–153. [CrossRef]
5. Wang, Y.; Cao, Z.; Au, S.-K. Efficient Monte Carlo Simulation of Parameter Sensitivity in Probabilistic Slope Stability Analysis. *Comput. Geotech.* **2010**, *37*, 1015–1022. [CrossRef]
6. Vallejo, L.E. Interpretation of the Limits in Shear Strength in Binary Granular Mixtures. *Can. Geotech. J.* **2001**, *38*, 1097–1104. [CrossRef]
7. Hu, J.; Weng, X.; Yang, L.; Lei, S.; Niu, H. Centrifugal Modeling Test on Failure Characteristics of Soil-Rock Mixture Slope under Rainfall. *Eng. Fail. Anal.* **2022**, *142*, 106775. [CrossRef]
8. Curry, A.M.; Black, R. Structure, Sedimentology and Evolution of Rockfall Talus, Mynydd Du, South Wales. *Proc. Geol. Assoc.* **2003**, *114*, 49–64. [CrossRef]
9. Pande, G.N.; Pietruszczak, S.; Wang, M. Role of Gradation Curve in Description of Mechanical Behavior of Unsaturated Soils. *Int. J. Geomech.* **2020**, *20*, 04019159. [CrossRef]

10. Zhai, X.; Horn, R. Effect of Static and Cyclic Loading Including Spatial Variation Caused by Vertical Holes on Changes in Soil Aeration. *Soil Tillage Res.* **2018**, *177*, 61–67. [CrossRef]
11. Masoudian, M.S.; Zevgolis, I.E.; Deliveris, A.V.; Marshall, A.M.; Heron, C.M.; Koukouzas, N.C. Stability and Characterisation of Spoil Heaps in European Surface Lignite Mines: A State-of-the-Art Review in Light of New Data. *Environ. Earth Sci.* **2019**, *78*, 505. [CrossRef]
12. Cui, Y.; Chan, D.; Nouri, A. Coupling of Solid Deformation and Pore Pressure for Undrained Deformation-a Discrete Element Method Approach. *Int. J. Numer. Anal. Methods Geomech.* **2017**, *41*, 1943–1961. [CrossRef]
13. Di Maio, C.; Vassallo, R. Geotechnical Characterization of a Landslide in a Blue Clay Slope. *Landslides* **2011**, *8*, 17–32. [CrossRef]
14. Wang, G.; Zhang, D.; Furuya, G.; Yang, J. Pore-Pressure Generation and Fluidization in a Loess Landslide Triggered by the 1920 Haiyuan Earthquake, China: A Case Study. *Eng. Geol.* **2014**, *174*, 36–45. [CrossRef]
15. Peruccacci, S.; Brunetti, M.T.; Gariano, S.L.; Melillo, M.; Rossi, M.; Guzzetti, F. Rainfall Thresholds for Possible Landslide Occurrence in Italy. *Geomorphology* **2017**, *290*, 39–57. [CrossRef]
16. Horacio, J.; Muñoz-Narciso, E.; Trenhaile, A.S.; Pérez-Alberti, A. Remote Sensing Monitoring of a Coastal-Valley Earthflow in Northwestern Galicia, Spain. *CATENA* **2019**, *178*, 276–287. [CrossRef]
17. He, L.; Francioni, M.; Coggan, J.; Calamita, F.; Eyre, M. Modelling the Influence of Geological Structures in Paleo Rock Avalanche Failures Using Field and Remote Sensing Data. *Remote Sens.* **2022**, *14*, 4090. [CrossRef]
18. Geertsema, M.; Menounos, B.; Bullard, G.; Carrivick, J.L.; Clague, J.J.; Dai, C.; Donati, D.; Ekstrom, G.; Jackson, J.M.; Lynett, P.; et al. The 28 November 2020 Landslide, Tsunami, and Outburst Flood—A Hazard Cascade Associated With Rapid Deglaciation at Elliot Creek, British Columbia, Canada. *Geophys. Res. Lett.* **2022**, *49*, e2021GL096716. [CrossRef]
19. Sanz de Ojeda, P.; Sanz Pérez, E.; Galindo, R.; Sanz Riaguas, C. Retrospective Modeling of a Large Paleo-Landslide Related to Deglaciation in the Sierra de Urbión, Cordillera Ibérica, Spain. *Appl. Sci.* **2021**, *11*, 4277. [CrossRef]
20. Wang, J.-J.; Liang, Y.; Zhang, H.-P.; Wu, Y.; Lin, X. A Loess Landslide Induced by Excavation and Rainfall. *Landslides* **2014**, *11*, 141–152. [CrossRef]
21. Troncone, A.; Pugliese, L.; Conte, E. Analysis of an Excavation-Induced Landslide in Stiff Clay Using the Material Point Method. *Eng. Geol.* **2022**, *296*, 106479. [CrossRef]
22. Zhang, Y.; Zhang, J.; Chen, G.; Zheng, L.; Li, Y. Effects of Vertical Seismic Force on Initiation of the Daguangbao Landslide Induced by the 2008 Wenchuan Earthquake. *Soil Dyn. Earthq. Eng.* **2015**, *73*, 91–102. [CrossRef]
23. Bojadjieva, J.; Sheshov, V.; Bonnard, C. Hazard and Risk Assessment of Earthquake-Induced Landslides—Case Study. *Landslides* **2018**, *15*, 161–171. [CrossRef]
24. Hoek, E.; Bray, J.W. *Rock Slope Engineering*, 3rd ed.; The Institute of Mining and Metallurgy: London, UK, 1981.
25. Taylor, D.W. Stability of Earth Slopes. *J. Boston Soc. Civ. Eng.* **1937**, *24*, 197–247.
26. Bishop, A.W. The Use of the Slip Circle in the Stability Analysis of Slopes. *Géotechnique* **1955**, *5*, 7–17. [CrossRef]
27. Spencer, E. A Method of Analysis of the Stability of Embankments Assuming Parallel Inter-Slice Forces. *Géotechnique* **1967**, *17*, 11–26. [CrossRef]
28. VandenBerge, D.R.; Duncan, J.M.; Brandon, T.L. Limitations of Transient Seepage Analyses for Calculating Pore Pressures during External Water Level Changes. *J. Geotech. Geoenvironmental Eng.* **2015**, *141*, 04015005. [CrossRef]
29. Prakasam, C.; Aravinth, R.; Nagarajan, B.; Kanwar, V.S. Site-Specific Geological and Geotechnical Investigation of a Debris Landslide along Unstable Road Cut Slopes in the Himalayan Region, India. *Geomat. Nat. Hazards Risk* **2020**, *11*, 1827–1848. [CrossRef]
30. Dastpak, P.; Jamshidi Chenari, R.; Cami, B.; Javankhoshdel, S. Noncircular Deterministic and Stochastic Slope Stability Analyses and Design of Simple Geosynthetic-Reinforced Soil Slopes. *Int. J. Geomech.* **2021**, *21*, 04021155. [CrossRef]
31. Stead, D.; Wolter, A. A Critical Review of Rock Slope Failure Mechanisms: The Importance of Structural Geology. *J. Struct. Geol.* **2015**, *74*, 1–23. [CrossRef]
32. Hammouri, N.A.; Malkawi, A.I.H.; Yamin, M.M.A. Stability Analysis of Slopes Using the Finite Element Method and Limiting Equilibrium Approach. *Bull. Eng. Geol. Environ.* **2008**, *67*, 471–478. [CrossRef]
33. Jian, W.; Wang, Z.; Yin, K. Mechanism of the Anlesi Landslide in the Three Gorges Reservoir, China. *Eng. Geol.* **2009**, *108*, 86–95. [CrossRef]
34. Liu, Y.; Zhang, W.; Zhang, L.; Zhu, Z.; Hu, J.; Wei, H. Probabilistic Stability Analyses of Undrained Slopes by 3D Random Fields and Finite Element Methods. *Geosci. Front.* **2018**, *9*, 1657–1664. [CrossRef]
35. Li, T.Z.; Yang, X.L. Stability of Plane Strain Tunnel Headings in Soils with Tensile Strength Cut-Off. *Tunn. Undergr. Space Technol.* **2020**, *95*, 103138. [CrossRef]
36. Thimpson, M.; Harding, S.H.; Finey, J.; Vaughan, P.; Briggs, W.; Brown, R.; Rodin, S.; Cochrane, N.; Bishop, A.; Humphreys, J.; et al. DISCUSSION. COLLIERY SPOIL TIPS—AFTER ABERFAN. (ORIGINAL PAPER PUBLISHED AS A SEPARATE DOCUMENT—LOAN COPIES AT 7598). *Proc. Inst. Civ. Eng.* **1973**, *55*, 677–712.
37. Forrester, D.J.; Whittaker, B.N. Effects of Mining Subsidence on Colliery Spoil Heaps. *Int. J. Rock Mech. Min. Sci. Geomech. Abstr.* **1976**, *13*, 113–120. [CrossRef]
38. Woodland, A.W.; Evan, W.B. The Geology of the South Wales Coalfield-Part 6. In *Memoirs of The Geological Survey of Great Britain*, 3rd ed.; London Her Majesty's Stationery Office: London, UK, 1964.
39. Met Office Hadley Centre. *Data: Variables from HadUK-Grid over UK for Daily Data*; Met Office Hadley Centre: Exeter, UK, 2023.

40. Welsh Government. DataMapWales. Available online: https://datamap.gov.wales/ (accessed on 2 April 2023).
41. Taylor, R.K. English and Welsh Colliery Spoil Heaps—Mineralogical and Mechanical Interrelationships. *Eng. Geol.* **1975**, *9*, 39–52. [CrossRef]
42. Holubec, I. Geotechnical Aspects of Coal Waste Embankments. *Can. Geotech. J.* **1976**, *13*, 27–39. [CrossRef]
43. Bentley, S.P.; Davies, M.C.R.; Gallup, M. The Cilfynydd Flow Slide of December 1939. *Q. J. Eng. Geol. Hydrogeol.* **1998**, *31*, 273–289. [CrossRef]
44. Davies, M.C.R.; Johnston, A.G.; Williams, K.P. Stabilised Mixed Colliery Spoil in Land Reclamation. *Int. J. Surf. Min. Reclam. Environ.* **1998**, *12*, 1–4. [CrossRef]
45. Okagbue, C.O. The Geotechnical Characteristics and Stability of a Spoil Heap at a Southwestern Pennsylvania Coal Mine, U.S.A. *Eng. Geol.* **1984**, *20*, 325–341. [CrossRef]
46. Amos, P.W.; Younger, P.L. Substrate Characterisation for a Subsurface Reactive Barrier to Treat Colliery Spoil Leachate. *Water Res.* **2003**, *37*, 108–120. [CrossRef]
47. Rocscience. Slide3 | 3D Slope Stability Analysis Software—Rocscience. Available online: https://www.rocscience.com/software/slide3 (accessed on 5 April 2023).
48. Collin, J.G.; Stark, T.D.; Lucarelli, A.; Taylor, T.P.; Berg, R.R. Stability and Stress-Deformation Analyses of Reinforced Slope Failure at Yeager Airport. *J. Geotech. Geoenviron. Eng.* **2021**, *147*, 04020179. [CrossRef]
49. Firincioglu, B.S.; Ercanoglu, M. Insights and Perspectives into the Limit Equilibrium Method from 2D and 3D Analyses. *Eng. Geol.* **2021**, *281*, 105968. [CrossRef]
50. Lashgari, M.; Ozturk, C.A. Slope Failure and Stability Investigations for an Open Pit Copper Mine in Turkey. *Environ. Earth Sci.* **2022**, *81*, 5. [CrossRef]
51. Janbu, N. Application of Composite Slip Surfaces for Stability Analysis. In Proceedings of the European Conference on Stability of Earth Slopes, Stockholm, Sweden, 20–25 September 1954; pp. 43–49.
52. Itasca Consulting Group Inc. FLAC3D | US Minneapolis—Itasca Consulting Group, Inc. Available online: https://www.itascacg.com/software/FLAC3D (accessed on 16 April 2023).
53. Yang, X.; Hou, D.; Tao, Z.; Peng, Y.; Shi, H. Stability and Remote Real-Time Monitoring of the Slope Slide Body in the Luoshan Mining Area. *Int. J. Min. Sci. Technol.* **2015**, *25*, 761–765. [CrossRef]
54. Yin, Y.; Li, B.; Wang, W. Dynamic Analysis of the Stabilized Wangjiayan Landslide in the Wenchuan Ms 8.0 Earthquake and Aftershocks. *Landslides* **2015**, *12*, 537–547. [CrossRef]
55. Dong, J.; Yang, X.; Yang, J.; Wang, C. Formation Mechanism and Failure Analysis under Fluctuating Reservoir Water Level Conditions of a Large-Scale Accumulation Slope. *Bull. Eng. Geol. Environ.* **2022**, *81*, 181. [CrossRef]
56. Gallage, C.; Uchimura, T. Direct Shear Testing on Unsaturated Silty Soils to Investigate the Effects of Drying and Wetting on Shear Strength Parameters at Low Suction. *J. Geotech. Geoenviron. Eng.* **2016**, *142*, 04015081. [CrossRef]
57. Lei, X.; Yang, Z.; He, S.; Liu, E.; Wong, H.; Li, X. Numerical Investigation of Rainfall-Induced Fines Migration and Its Influences on Slope Stability. *Acta Geotech.* **2017**, *12*, 1431–1446. [CrossRef]
58. Rahardjo, H.; Nio, A.S.; Leong, E.C.; Song, N.Y. Effects of Groundwater Table Position and Soil Properties on Stability of Slope during Rainfall. *J. Geotech. Geoenviron. Eng.* **2010**, *136*, 1555–1564. [CrossRef]
59. Ray, R.L.; Jacobs, J.M.; De Alba, P. Impacts of Unsaturated Zone Soil Moisture and Groundwater Table on Slope Instability. *J. Geotech. Geoenviron. Eng.* **2010**, *136*, 1448–1458. [CrossRef]
60. Peranić, J.; Mihalić Arbanas, S.; Arbanas, Ž. Importance of the Unsaturated Zone in Landslide Reactivation on Flysch Slopes: Observations from Valići Landslide, Croatia. *Landslides* **2021**, *18*, 3737–3751. [CrossRef]
61. Lowe, J.A.; Bernie, D.; Bett, P.; Bricheno, L.; Brown, S.; Calvert, D.; Clark, R.; Edwards, T.; Fosser, G.; Fung, F.; et al. UKCP18 Science Overview Report. 2018. Available online: https://www.metoffice.gov.uk/research/approach/collaboration/ukcp/science/science-reports (accessed on 21 May 2023).
62. Met Office Hadley Centre. *Data: Variables from Local Projections (2.2 km) Regridded to 5km over UK for Daily Data*; Met Office Hadley Centre: Exeter, UK, 2018.
63. Wang, H.; Zhang, Y.C.; Hu, H.Y. A Study on Relationship of Landslide Occurrence and Rainfall. *Appl. Mech. Mater.* **2013**, *438–439*, 1200–1204. [CrossRef]
64. Chinkulkijniwat, A.; Salee, R.; Horpibulsuk, S.; Arulrajah, A.; Hoy, M. Landslide Rainfall Threshold for Landslide Warning in Northern Thailand. *Geomat. Nat. Hazards Risk* **2022**, *13*, 2425–2441. [CrossRef]
65. Matsushi, Y.; Matsukura, Y. Cohesion of Unsaturated Residual Soils as a Function of Volumetric Water Content. *Bull. Eng. Geol. Environ.* **2006**, *65*, 449–455. [CrossRef]
66. Ahmadi Naghadeh, R.; Toker, N.K. Exponential Equation for Predicting Shear Strength Envelope of Unsaturated Soils. *Int. J. Geomech.* **2019**, *19*, 04019061. [CrossRef]